High-Resolution Electron Microscopy Study of ZSM-12 (MTW)

S. Ritsch,*[,†,‡] N. Ohnishi,[‡] T. Ohsuna,[‡] K. Hiraga,[‡] O. Terasaki,*[,†,§] Y. Kubota,[||] and Y. Sugi[||]

CREST, Japan Science and Technology Corporation (JST), Japan, Institute for Materials Research and Department of Physics, Graduate School of Science and Center for Interdisciplinary Research, Tohoku University, Sendai 980-8577, Japan, and Department of Chemistry, Faculty of Engineering, Gifu University, Gifu 501-11, Japan

Received June 5, 1998. Revised Manuscript Received August 5, 1998

The effect of different structure-directing agents (SDAs) on the nucleation of MTW (the structure code for ZSM-12 recommended by the International Zeolite Association Structure Commission) is shown by means of transmission electron microscopy (TEM). A loose-fit SDA interacting only weakly with the framework seems to have pore-filling character only and results in large domains with rather perfect ZSM-12 framework structure. Conversely, a more tight-fit SDA interacts markedly with the framework during the crystallization and causes simultaneous growth of small domains as well as frequent twinning. By comparison of simulated and experimental electron diffraction patterns as well as high-resolution transmission electron microscopy (HRTEM) images, the proposed crystal structure of ZSM-12 is substantiated. The presence of an organic SDA confined in the one-dimensional channels is established in HRTEM images obtained from calcined as well as as-synthesized specimens. This result is corroborated not only by corresponding image contrast simulations, but also by a significant reduction in intensity of low-angle reflections in quantitative electron diffraction patterns obtained from the as-synthesized material.

Introduction

High-silica zeolites are materials of interest due to their catalytic and molecular sieve properties as well as to their capability of serving as host materials of nanometer-sized clusters. These properties are determined by the atomic structure of the framework as well as by the intermediate and long range arrangement of the structural units within the topology of this framework. The latter is often affected by extensive twinning or faulting in the materials which originates during the nucleation process and impedes the characterization of the framework structure. Such twinning usually leads to different stacking sequences of two possible end-members of stacking polymorphs.

ZSM-12 is a high-silica zeolite first synthesized by Rosinski and Rubin.[1] It has a one-dimensional noninterpenetrating 12-membered ring pore system with a pore opening of approximately 5.6 Å × 7.7 Å.[2] A first proposal of the host framework topology was given by LaPierre et al.[3] on the basis of electron and X-ray powder diffraction combined with model building. Later the crystal structure was refined by Fyfe et al.[2] with the help of high-resolution solid-state NMR and synchrotron X-ray powder diffraction. They suggested that ZSM-12 crystallizes in a monoclinic structure with lattice parameters $a_0 = 24.863$ Å, $b_0 = 5.012$ Å, $c_0 = 24.328$ Å, and $\beta = 107.7°$ and the space group $C2/c$. Views of this unit cell along all three axes are shown in Figure 1. However, in both structural proposals it was pointed out that the structure is prone to make twinning with (100) twin planes. If one stacking layer is defined as the sheet between two adjacent (200) planes (see single stacking layer in Figure 2), this leads to two possible end members. One end member (monoclinic) is MTW (the structure code for ZSM-12 recommended by the International Zeolite Association Structure Commission). Polymorph A is formed by stacking in an abab... sequence (here stacking sheet b is a mirror image of sheet a, and thus, the channel position is shifted

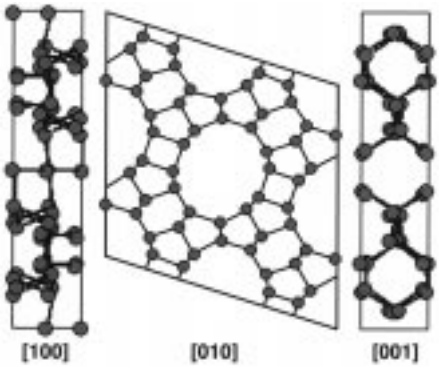

Figure 1. Unit cell of ZSM-12 viewed along the three main zone axes (polymorph B).

† CREST, Japan Science and Technology Corp.
‡ Institute for Materials Research, Tohoku University.
§ Department of Physics, Tohoku University.
|| Gifu University.

(1) Rosinski, E. J.; Rubin, M. K. US Patent 3,832,449, 1974.
(2) Fyfe, C. A.; Gies, H.; Kokotailo, G. T.; Marler, B.; Cox, D. E. *J. Phys. Chem.* **1990**, *94*, 3718.
(3) LaPierre, R. B.; Rohrmann, A. C.; Schlenker, J. L.; Wood, J. D.; Rubin, M. K.; Rohrbaugh, W. J. *Zeolites* **1985**, *5*, 3346.

10.1021/cm980410a CCC: $15.00
Published on Web 11/04/1998

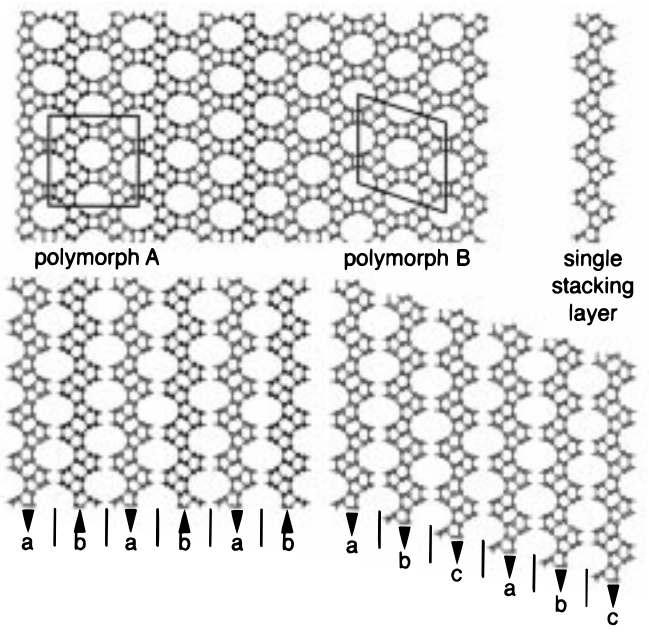

Figure 2. Framework structure of the two end-member polymorphs of the MTW zeolite family, viewed along the 12-membered ring pores. A single stacking sheet as well as the different arrangement of the sheets in the two polymorphs are shown.

upward and downward alternately by one-third of the channel distance; Figure 2). For polymorph B, the stacking sequence is abcabc... (here each consecutive stacking layer a, b, c is shifted downward by one-third of the channel distance; Figure 2). While the proposed framework of ZSM-12 represents the monoclinic polymorph B, twinning at every stacking sheet results in the orthorhombic polymorph A, which defines a new structure type (with space group *Pmcn* and lattice parameters $a_0 = 24.30$ Å, $b_0 = 23.70$ Å, $c_0 = 5.01$ Å), as already pointed out in refs 2 and 3. In Figure 2, the twinning together with outlines of a single stacking sheet as well as the unit cells for both polymorphs is depicted. In all the literature about MTW, it is stated that an undetermined amount of twinning was present in the examined samples.

A system in which similar stacking polymorphs and the control of their probability by mixture of different structure-directing agents (SDAs) have extensively been studied is the family of CIT-1, SSZ-26, and SSZ-33. While CIT-1 is a pure end-member polymorph B, SSZ-33 and SSZ-26 are disordered materials formed mostly of the polymorph B, but with fault probabilities of 30% and 15%, respectively.[4,5]

Here, we have studied samples of MTW synthesized with different organic SDAs, which are supposed to affect in different ways the organic−silica interaction during the nucleation of the framework, by means of high-resolution transmission electron microscopy (HRTEM) and electron diffraction (ED). The present study is focused on two MTW samples (S1 and S2) synthesized with a loose-fit and a rather tight-fit SDA, respectively, while samples obtained from SDAs of other sizes were

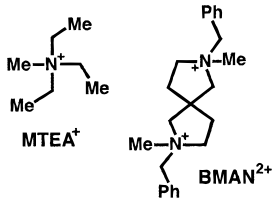

Figure 3. Structure of the SDAs used in synthesis: $MTEA^+$ (S1) and $BMAN^{2+}$ (S2).

only examined for sake of consistency with the present results. (With the term "fit" we also want to express the strength of the organic−silica interaction of the SDAs during the nucleation process.) First the influence of these different SDAs on the structure and possible twinning in MTW are examined. Next, the structure models suggested by Fyfe et al.[2] and LaPierre et al.[3] are investigated in terms of ED and by comparison of HRTEM images with corresponding image contrast simulations. Finally, we show that the presence of an organic SDA in the structure can be manifested by HRTEM as well as ED.

Experimental Section

Synthesis and Analysis. The two different all-silica MTW samples (S1 and S2) were synthesized using two organic SDAs assumed (from their geometries; see Figure 3) to have different interaction with the framework structure. S1 was synthesized using triethylmethylammonium bromide ($MTEA^+Br^-$).[6] The hydrothermal synthesis was carried out statically with SiO_2:$MTEA^+Br$:$NaOH$:H_2SO_4:H_2O = 1:0.43:0.64:0.195:50 at 150 °C for 10 days. For the synthesis of S2, 2,7-dibenzyl-2,7-dimethyl-2,7-diazoniaspiro[4.4]nonane dihydroxide [$BMAN^{2+}(OH^-)_2$] was used, which is a new SDA obtained from malononitrile in six steps.[7] The hydrothermal synthesis was carried out statically with SiO_2:$BMAN^{2+}(OH^-)_2$:$NaOH$:H_2O = 1:0.1:0.1:50 at 150 °C for 12 days. More details on the synthesis of the SDAs and the zeolite samples will be described elsewhere. As-synthesized samples were analyzed and confirmed to be pure MTW by X-ray powder diffraction, thermogravimetric analysis, nuclear magnetic resonance spectroscopy, and scanning electron microscopy.[7]

High-Resolution Electron Microscopy and Electron Diffraction. The specimens for TEM were prepared from powders of samples by conventional crushing in an agate mortar and dispersing the resulting small crystallites onto a holey carbon foil supported by a Cu grid. All TEM observations were performed with a 400 kV (JEM 4000EX) electron microscope (point resolution 1.7 Å) equipped with a slow-scan CCD camera (Gatan model 694). HRTEM images were recorded on high-sensitivity photographic films (in order to use low-dose imaging conditions and, thus, not to damage the zeolite material quickly, but to still have the benefits of the high resolution of a photographic film). Most of the ED patterns were acquired with the CCD camera, which has the advantage of a linear intensity response compared to the photographic film. This is necessary, if the ED patterns are to be analyzed quantitatively. During recording of the ED patterns, the beam intensity was reduced to a minimum, so that the intensity distribution of the patterns did not change throughout the observation process due to irradiation damage. The patterns were recorded from small regions near very thin edges of crystallites. In this case, kinematical scattering can be assumed, since the all-silica zeolite material contains only very weak scatterers. Image contrast calculations were performed according to the multislice algorithm with the MacTem-

(4) Lobo, R. F.; Zones, S. I.; Davis, M. E. *Stud. Surf. Sci. Catal.* **1994**, *84*, 461.
(5) Lobo, R. F.; Pan, M.; Chan, I.; Medrud, R. C.; Zones, S. I.; Crozier, P. A.; Davis, M. E.; *J. Phys. Chem.* **1994**, *98*, 12040.
(6) Ernst, S.; Jacobs, P. A.; Martens, J. A.; Weitkamp, J. *Zeolites* **1987**, *7*, 458.
(7) Kubota, Y.; Seriu, A.; Moriyama, Y.; Sugi, Y.; Ritsch, S.; Hiraga, K.; Terasaki, O., Proceedings of IZC12, Baltimore, July 5−10, 1998.

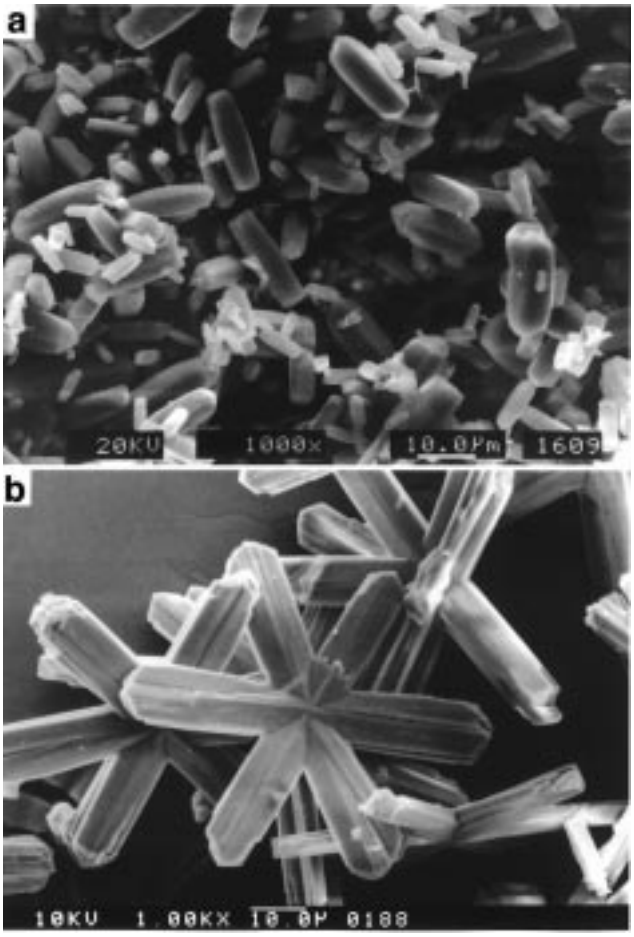

Figure 4. Scanning electron micrographs showing morphologies and crystal sizes for as-synthesized S1 (a) and S2 (b).

pas software. All Fourier image filtering of HRTEM micrographs was performed with the Gatan DigitalMicrograph 2.5 software.

Results and Discussion

Nucleation and Twinning. Parts a and b of Figure 4 show scanning electron micrographs of the samples S1 and S2, respectively. While S1 consists of elongate and very smooth crystallites of up to 20 μm in length and 8 μm in diameter, for S2 mainly planar pseudo-six-fold stars with branches being a little larger than the S1 crystallites are found. The surface morphology of these stars suggests that they are formed by subgrains.

In Figure 5a, a HRTEM image taken along the direction of the one-dimensional channels [010] of S1 is presented. A rather perfect framework structure extending over a large region can be seen, except for some subgrain boundaries, such as an antiphase−domain boundary along the lower part of the image (indicated by a series of arrows). It is suggested that in this case a weak organic−silica interaction may have caused slow nucleation and an according growth of large polymorph B domains. This can be assumed to result from $MTEA^+$ fitting only loosely into the ZSM-12 pores, since the molecule is relatively small and flexible (molecular modeling approximately yields a diameter of 6.7 Å and a length of 8.9 Å). $MTEA^+$ is suggested to suffer from Hofmann degradation, and the relatively high amount of sodium ions may additionally have weakened the structure directing effect so that it has a pore-filling character rather than a structure directing one.[7,8] By contrast, $BMAN^{2+}$ is bulky and relatively rigid (approximately 7.4 Å in diameter and 19.4 Å in length obtained from molecular modeling). It fits more tightly into the pores and, additionally, has intermediate hydrophobicity, which is very important to structure-direct high-silica zeolites.[9] As a consequence, there should be a noticeable organic−silica interaction of $BMAN^{2+}$ with the framework during the crystallization of ZSM-12, which is also effective over a long range due to the length of the organic molecule. Figure 5b has been obtained from sample S2 along the channel direction. Besides some twinning with (100) twin planes (indicated by arrows pointing along some of the twin boundaries), several grain boundaries separating the crystallite into quite small subgrains can be seen. It should be noted that most of the twin boundaries start at the grain boundaries, which are not smooth. The presence of many small subgrains can be interpreted as originating from a nucleation that starts simultaneously at many different positions within the gel due to a marked organic−silica interaction,[7] as described above. From the present observation, we may now speculate about the origin of the twinning in this sample: during the further nucleation process many of the subgrains crystallize with a common pore direction. However, due to the nonsmooth grain boundaries, which in Figure 5b do not correspond to low order crystal orientations, frequent twinning is caused along these grain boundaries to make up for the misfit of orientation along the grain boundaries (such twinning should be energetically favorable to other possible defects in the pure polymorph B). This offers possible explanations for the observed macroscopical surface morphologies. The growth velocity along the direction of the channels must be higher, since it was found that the channel direction corresponds to the long axis of the crystallites in both cases in Figure 4 (and also for the additional samples examined). Hence, the platelike morphology of the branches of the star can be understood as caused by different domains having grown rapidly in this direction. (Such a platelike morphology was also observed for other MTW samples obtained from rather large SDAs.) The approximate angles between the branches of the stars are $4 \times 64-66°$ and $2 \times 50-51°$, with opposing ones being equal. Yet, it should be mentioned that the origin of the "planar six-fold stars" is not clear. On the other hand, the smooth morphology of S1 (see Figure 4a) has its foundation in the microscopic structure observed for this sample consisting of very large domains.

A study involving a series of SDAs of different size and fitting into the pores of MTW is currently in preparation in order to clarify the effect of the organic−silica interaction during the nucleation of this zeolite. First results showed that a sample gained from a SDA with a size and interaction intermediate to those of S1 and S2 has structural features between these two samples. It contains a lower amount of twinning and

(8) Davis, M. E.; Zones, S. I. in *Synthesis of Microporous Materials: Zeolites, Clays and Nanostructures;* Occeli, M. L., Kessler, H., Eds.; Marcel Dekker: New York, 1996; Vol. 6, p 213.

(9) Kubota, Y.; Helmkamp, M. M.; Zones, S. I.; Davis, M. E. *Microspor. Mater.* **1996**, *6*, 213.

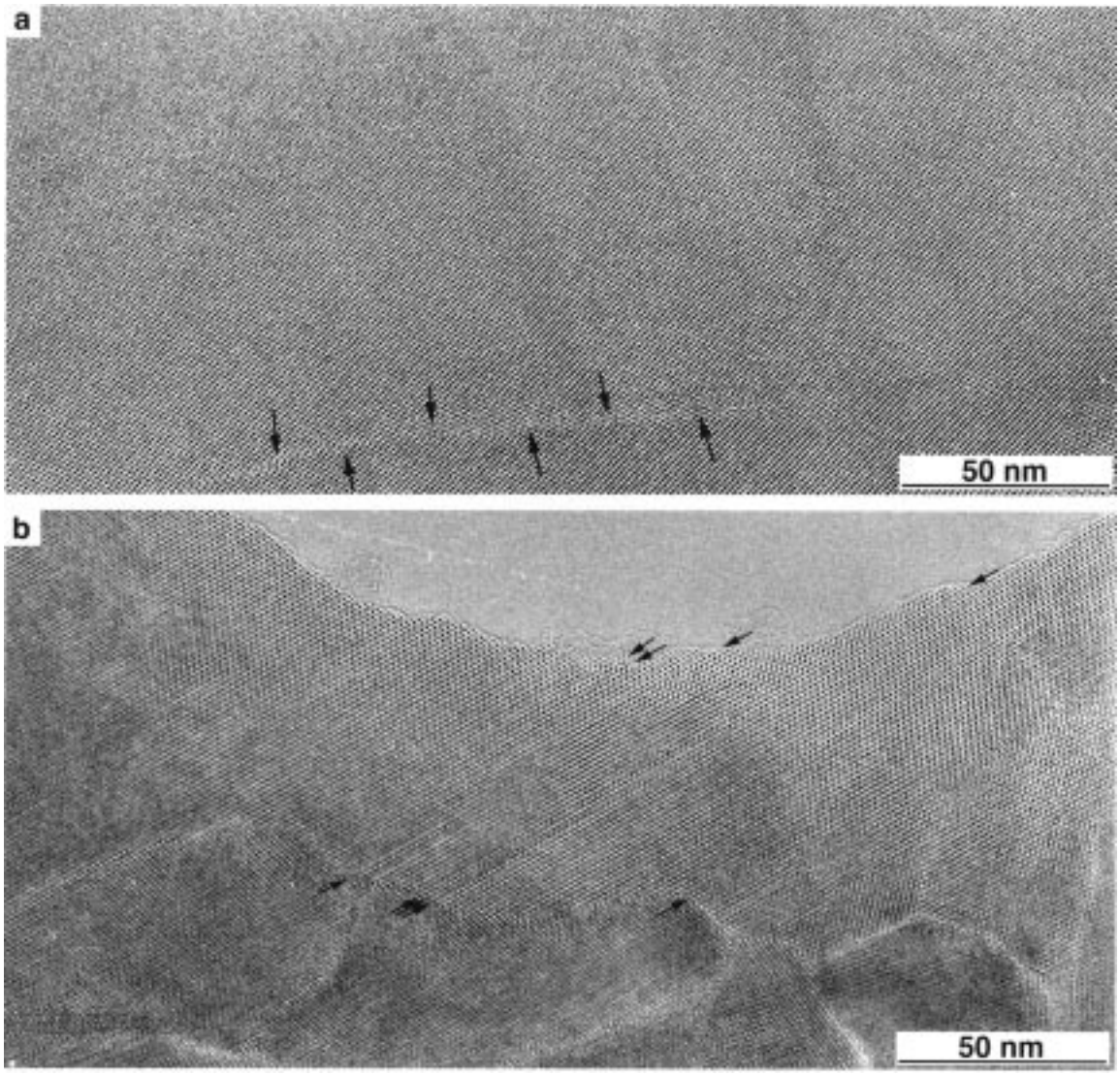

Figure 5. HRTEM images taken along the pore direction for as-synthesized samples S1 (a) and S2 (b). Arrows mark an antiphase boundary in panel a and point along twin boundaries in panel b.

larger subgrains than S2. A sample synthesized with a SDA even slightly larger than the one used for S2 again consisted of very small subgrains. Yet, no twinning was found to be present in that case. However, the existence of many and small subgrains may be an indicator for the strength of the organic−silica interaction.

Figure 6, another micrograph taken from S2 along the channel direction, shall be used for a more intense study of the nature of the twin boundaries and domains in this sample. Four square regions, marked by I to IV in the upper part of the figure, are displayed below the main image in higher magnification together with corresponding Fourier filtered images. These highlight different characteristics of the twinning. (For the sake of clarity, the twin boundaries are additionally indicated by arrowheads in the filtered images.) In the filtering process, circular masks were applied including only the pair of reflections split by twinning, which corresponds to the change of direction of the lattice fringes in the [100] direction. The regions II and IV represent the continuations of the regions I and III, respectively. In II, as well as the lower half of IV, only a single sharp twin boundary is present with large polymorph B domains on both sides. However, the filtered images of IV as well as the right half of II reveal that the layer sheets immediately accompanying the boundary suffer from a slight stress caused by the change in twinning of the adjacent regions in I and III, respectively. By contrast, some of the twin domains in other regions consist of only one stacking sheet, giving rise to small polymorph A domains. In I such a region can be seen. However, it disappears in its continuation into II. III depicts a region in which four neighboring twin boundaries split into two separated bundles, creating another twin domain between them (see IV). At the location of this splitting, a small polymorph A region is present. The product of the splitting is found in IV: while the lower twin boundary of the new domain is sharp, the upper boundary includes a single polymorph A sheet. The splitting additionally caused a shift downward by one sheet of the lower twin boundary.

Electron Diffraction. ED patterns from fragments of the crystallites of both samples were recorded under the precautions described in the Experimental Section. The upper row in Figure 7 displays calculated ED patterns along some main zone axes based on the model refined by Fyfe et al.;[2] in the lower row the correspond-

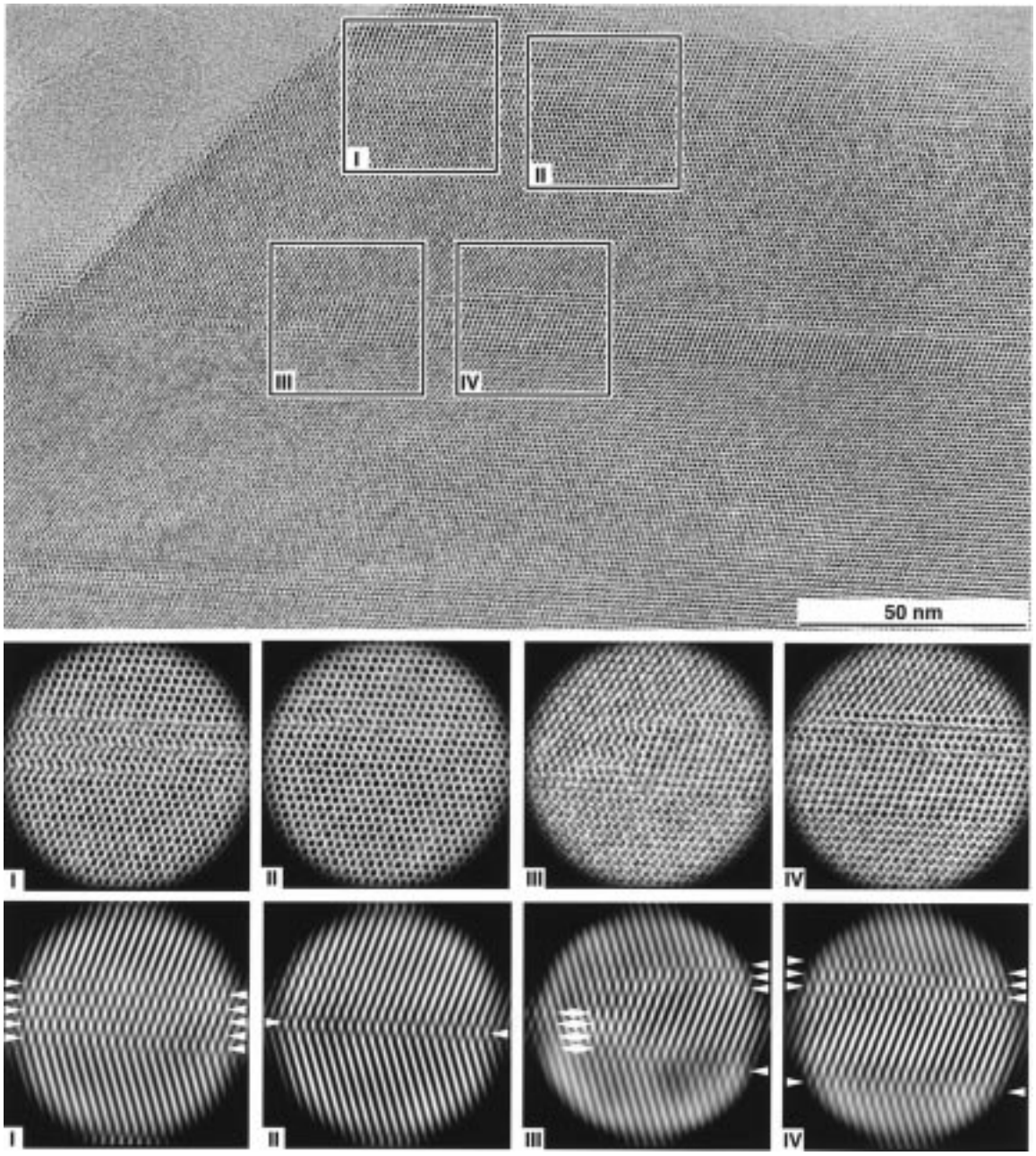

Figure 6. HRTEM image of S2 with [010] beam incidence. The four square regions I−IV are displayed below in higher magnification together with corresponding Fourier-filtered images highlighting different twinning features. In the latter the positions of the twin boundaries are indicated by arrowheads.

ing observed patterns are shown. In the patterns along [010] as well as [001], a very good match of calculated and observed patterns is found in terms of extinctions and intensity distribution of the reflections. The pattern along [100] is of great importance, since this is the only of the three main zone axes that yields evidence for the doubling of the *c*-axis parameter, as claimed in the structure model by Fyfe et al.[2] Furthermore, it should be noted that in the calculated pattern an extinction of layers with $l = 2n$ is present according to the structure model. Consequently, a lot of effort was made to acquire this axis. Unfortunately, only zone axes close to this [100] direction could be obtained experimentally. The fact that it was not possible to make experimental access to this axis can only be accounted for by a very low cleavage probability (for samples S1 and S2) of the structure perpendicular to [100] as compared to [010] and [001]. Yet, the patterns of the [110] direction presented in Figure 7 do also contain the additional spots indicating the *c*-axis doubling, since [110] is rather close to [100] for the present structure (some of these additional spots are marked by arrows in both patterns).

Different from these results, calculated [100] and [110] ED patterns based on the model by LaPierre et al.[3] do not show the additional spots that are the evidence for the *c*-axis doubling in the model by Fyfe et al.[2] A close look at the two structure models does not reveal an obvious difference. Actually, the *c*-doubling is manifested in small shifts of a few atoms only.[10]

Unlike the case of CIT-1, SSZ-33, and SSZ-26 mentioned above,[4,5] twinning occurs in a very inhomogeneous manner in the present case of S2. Besides the

(10) Gies, H., private communication.

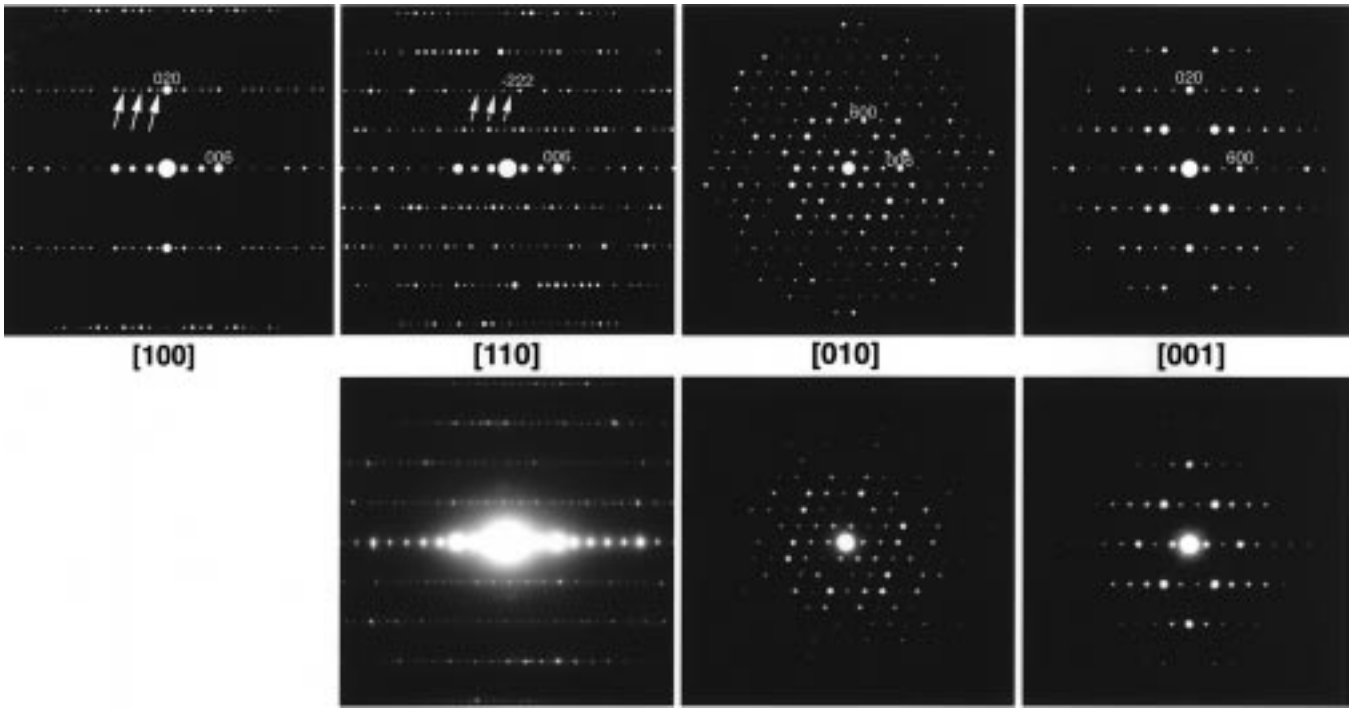

Figure 7. ED patterns along major zone axes obtained from single domains of ZSM-12: upper row, calculated; lower row, experimental (for details see the text).

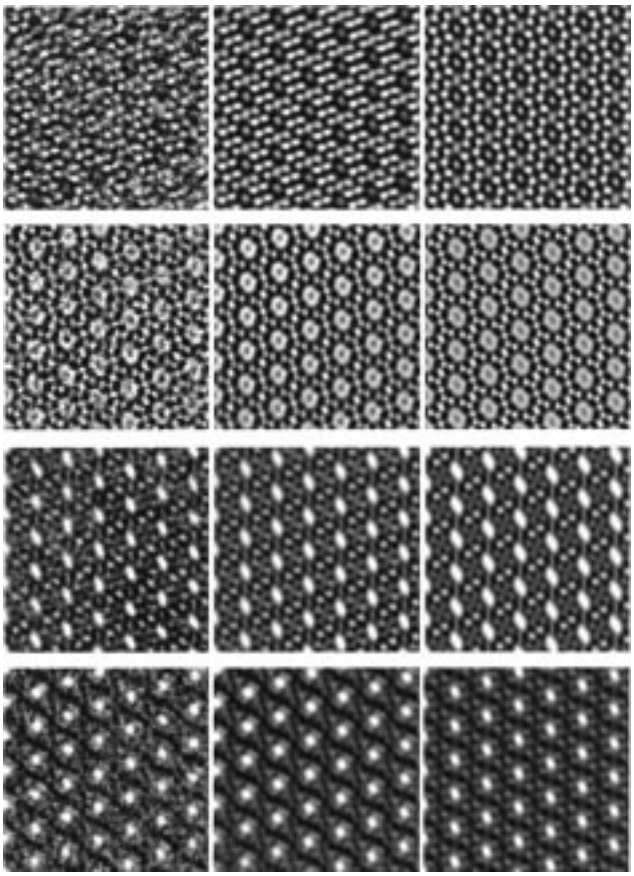

Figure 8. [010] HRTEM images for 50, −50, −110, and −155 nm defocus (top to bottom), respectively, shown as original (left), noise-filtered (middle), and simulated (right) micrographs.

frequent creation and extinction of twin boundaries as discussed for the region III in Figure 6, the presence of many domains of different sizes prohibits a quantitative statement on the twinning probability. Moreover, the occurrence of intergrowths of complete polymorph A domains is extremely rare compared to that of single twin boundaries (see Figures 5 and 6).

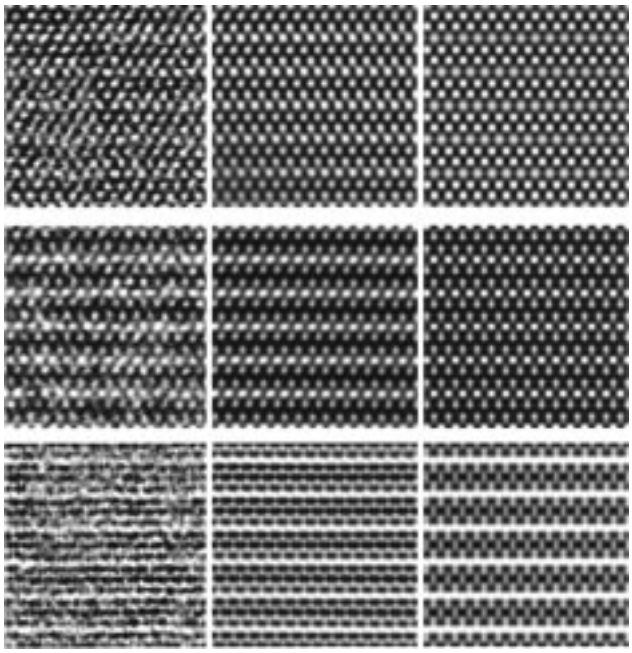

Figure 9. [001] HRTEM images as in Figure 8 for −50, −100, and +210 nm, respectively.

HRTEM and Image Contrast Simulation. In this paragraph we discuss the framework structure model for ZSM-12. As mentioned above, the difference between the model structure of La Pierre et al.[3] and the one of Fyfe et al.[2] is found in small shifts of a few atoms only. Even though these shifts result in the clear evidence in ED of the *c*-doubling for the Fyfe et al.[2] model, they are much too small to be detected by high-resolution imaging. Thus, HRTEM results cannot give any hint of the cell doubling. Accordingly, materials of

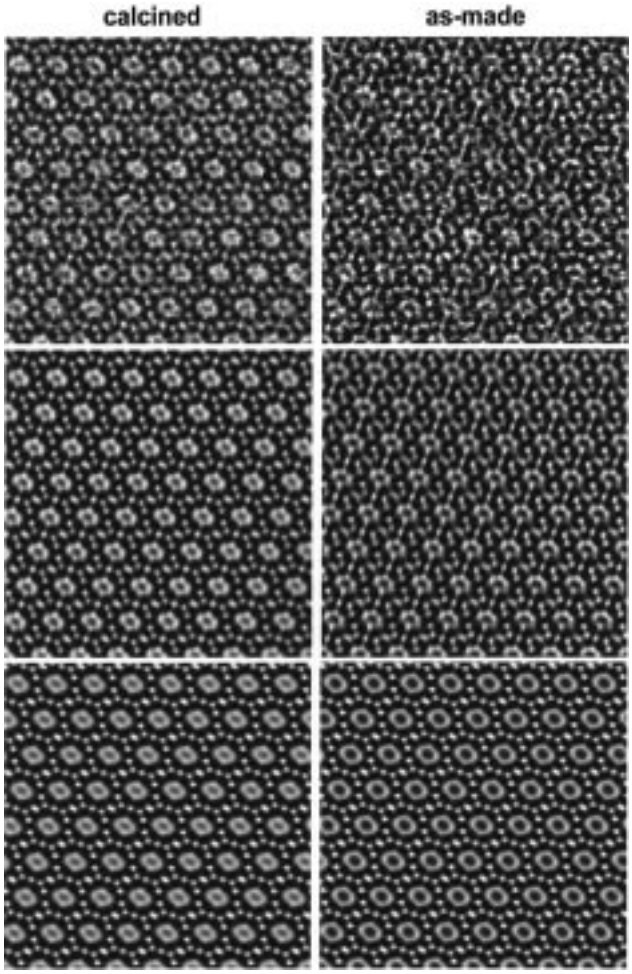

Figure 10. HRTEM images along [010], showing the difference of the contrast inside the pores for calcined (left) and as-synthesized (right) material for S2; from top to bottom: original, noise-filtered, and simulated images, respectively.

both model structures would yield the same HRTEM results. As a consequence, only the model by Fyfe et al.,[2] which has by ED been manifested, will be investigated in the following.

HRTEM micrographs showing series of defoci obtained from very thin specimen regions not containing any twinning are compared with images simulated from the Fyfe et al.[2] model. To facilitate the comparison of experimental and simulated images, the originally obtained micrographs were subjected to Fourier filtering to reduce the background noise, which is very high due to the weak-beam imaging conditions. The image-filtering process is based on an inverse Fourier transform of the power spectrum of the original image after applying circular mask filters on the diffraction spots.

A series of micrographs taken along the channel direction [010] with different defocus values is displayed in Figure 8 as original (left), noise filtered (middle), and simulated (right) images with the following defocus values from top to bottom: 50, −50, −110, and −155 nm. (Scherzer defocus for the JEM 4000EX is −48 nm.) For the calculated images, a specimen thickness of 40 Å was used. A good visual match is found between the filtered and the simulated images. Yet, it should be noted that in the experimental images at approximately 50 and −155 nm defocus a slight misalignment of the zone axis to the incident beam direction existed. This

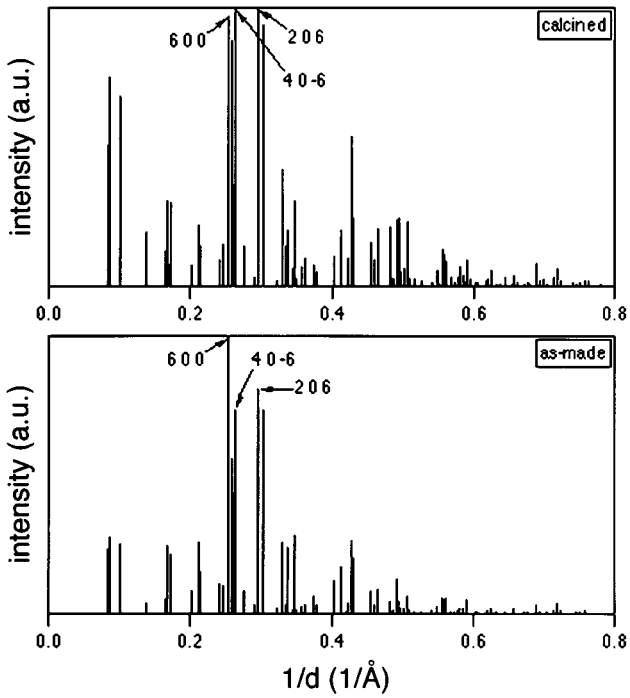

Figure 11. Distribution of normalized electron diffraction intensities vs space frequencies obtained from calcined and as-synthesized MTW zeolites, respectively.

is evident, for example, from the slight displacement of the bright dot inside the channel at 50 nm defocus in the filtered image. In Figure 9, a similar series of images along [001] is shown in the same manner as in Figure 8 (from top to bottom: −50, −100, and 210 nm defocus). Images simulated for a specimen thickness of approximately 50 Å resulted in the best match in this case. Due to the good agreement of simulated and noise-filtered images in both figures, the framework structure model of ZSM-12 suggested by Fyfe et al. could be substantiated. (It should be mentioned here that this result also shows the approximate validity of the framework structure as given by LaPierre et al.[3] considering the arguments at the beginning of this paragraph.)

Effect of a SDA Confined inside the Channels on HRTEM and ED Observations. For the primary investigations of the twinning, mainly the as-synthesized material still containing the organic SDAs inside the channels was used, since such material proved to have an increased stability under the electron beam. (It was our impression that increasing the size of the SDA and increasing the organic−silica interaction also increased the stability of the material under the beam.) Corresponding HRTEM studies revealed a very dark contrast at the center of the channels in images taken around the so-called optimum defocus. This has been reported to occur as an electron optical artifact imparted due to the insufficient transfer of some Bragg reflections during the imaging process of zeolite materials.[11,12] However, the dark contrast was extremely strong in the present case, and thus, a possible influence of the SDA

(11) Chan, I. Y.; Csencsits, R.; O'Keefe, M. A.; Gronsky, R. J. *J. Catal.* **1987**, *103*, 466.
(12) Alfredsson, V.; Terasaki, O.; Bovin, J.-O. *J. Solid State Chem.* **1993**, *105*, 223.

confined in the channels had to be assumed. In the following the results obtained for S2 are presented.

In the HRTEM observations, a difference in the contrast inside the one-dimensional channels could be established between as-synthesized and calcined samples. For images obtained close to the optimum defocus, the calcined samples show a very weak contrast inside the channels, while the presence of the organic SDA still confined within causes a very dark contrast there. This observation was confirmed by corresponding image contrast calculations. For these simulations, an approximate position of $BMAN^{2+}$ inside the pores was assumed. However, the presence of the SDA could only be manifested around this so-called optimum defocus of the objective lens of the microscope. For this specific defocus, a series of original, noise-filtered, and simulated images is presented in Figure 10 from top to bottom, respectively. Especially the noise-filtered as well as the simulated images clearly highlight the above-mentioned difference between material without (left) and with (right) SDA confined in the channels. Even though the image of the as-synthesized sample suffers from a slight misalignment of the zone axis to the incident beam, the contrast inside its pores is very dark compared to the calcined case. In fact, it is promising for future investigations that the presence of an organic—and thus very weakly scattering—material confined inside the pores could unambiguously be proven by HRTEM.

This result is corroborated by quantitative ED data obtained from the same samples. In [010] zone axis ED patterns, the intensities of the reflections with the shortest space frequencies, obtained from the calcined material, are reduced by a factor of approximately 3, compared to those of as-synthesized samples (Figure 11). This is in agreement with the assumption that those reflections, which correspond to the spacing of the pores, should be influenced most strongly by the presence of the organic SDA. Similar observations have already been reported for TPA^+ in MFI as well as MoS_2 in Na−FAU.[13,14] An attempt to use these ED data for a Fourier synthesis in order to clarify the crystallographic relation of the SDA inside the channels is now aimed for.

Acknowledgment. The authors greatly acknowledge CREST, Japan Science and Technology Corporation, for financial support. O.T. is also grateful for a Grant-in-Aid for Scientific Research in Priority Areas from the Ministry of Education, Science, Sport and Culture of Japan. We also thank A. Seriu and Y. Moriyama for technical assistance. Part of this work has been financially supported by the New Energy and Industrial Technology Development Organization (NEDO) of Japan and by the Foundation of Advanced Technology Institute.

CM980410A

(13) Ohnishi, N.; Hiraga, K. *J. Electron Microsc.* **1996**, *45*, 85.
(14) Ohnishi, N.; Ohsuna, T.; Sakamoto, Y.; Terasaki, O.; Hiraga, K. *Micropor. Mesopor. Mater.* **12998**, 21, 581.